This article has been accepted for inclusion in a future issue of this journal. Content is final as presented, with the exception of pagination.

Hovercraft Control With Dynamic Parameters Identification

David Cabecinhas, Pedro Batista, *Member, IEEE*, Paulo Oliveira, *Senior Member, IEEE*, and Carlos Silvestre, *Member, IEEE*

***Abstract*— This paper presents an integrated parameter estimator and trajectory tracking controller for a hovercraft. A generic parameter estimator for time-varying systems linear in the parameters is derived and then particularized for the dynamic model of the vehicle at hand. A trajectory tracking controller is proposed for the nonholonomic hovercraft, which renders the tracking error system exponentially stable and its zero dynamics stable. The interconnection of the estimator and the controller is proven to be locally asymptotically stable. Experimental results attesting the performance and robustness of the controller and its interconnection with the estimator are presented.**

***Index Terms*— Hovercraft, nonholonomic systems, parameter estimation, trajectory tracking.**

I. Introduction

NONLINEAR motion control of underactuated vehicles, and more specifically thrust propelled surface vehicles, as in the case of ships or hovercraft, is an active topic of research that raises new and challenging problems compared with motion control of its fully actuated counterpart.

Hovercraft are highly versatile and agile vehicles, easily deployable, and able to withstand motion on different surfaces. While these characteristics make them top choices in a myriad of difficult operation scenarios, they also pose additional challenging and interesting problems in automatic control. On the one hand, hovercraft are usually underactuated. On the other hand, their dynamics can change dramatically over time as the surface they dwell on varies.

Early work on the control of underactuated surface vehicles that are able to sideslip laterally can be found in [1], and the references within, wherein the authors proposed a position tracking controller for a hovercraft that was modeled from an underactuated ship with several simplifications such as neglecting drag, assuming a symmetric shape and considering that the propellers are located at the center of mass. The proposed controllers drive the position exponentially to zero but the surge and angular velocities are taken as input and the control laws are discontinuous. In [2], a bounded nonlinear controller is given for stabilization and tracking of a single vehicle using a cascade backstepping method. A bounded force controller is specified for the translational part of the hovercraft system and it is then backstepped through the angular dynamics resulting in a control law for the torque input. A controller for hovercraft position tracking that exponentially stabilizes the tracking error to an arbitrarily small neighborhood of the origin is proposed in [3]. The controller is based on nonlinear Lyapunov methods and the backstepping technique and hinges on driving the position error of a fixed point in the vehicle frame of reference to zero, to avoid the introduction of singularities. Nonclassical controllers such as fuzzy controllers have also been proposed for trajectory tracking of hovercraft-like vehicles, such as the switching fuzzy controller developed in [4], but the authors only consider straight line trajectories and do not regulate the velocity. The University of Illinois has a testbed for networked and decentralized control comprised of multiple small hockey puck-like hovercraft [5]. Each hovercraft has four thrusters that are able to generate lateral force in any direction and a fifth one for providing lift. The individual vehicle trajectory controllers make use of a multirate nonlinear filtering and control algorithm that improves on an LQR tracking controller but position errors are still noticeable. More recently, multivariable nonlinear quantitative feedback theory was used in [6] to design a tracking controller for a hovercraft with uncertainty in the model parameters. The proposed controller is robust to uncertain parameters in the model but relies on local linearization of the nonlinear plant.

In this paper, we propose to design and experimentally validate a nonlinear controller for a hovercraft based on Lyapunov methods. The hovercraft model we consider is actuated through thrust force and rudder angle and subject to static and linear velocity drag forces. This structure induces lateral forces on the vehicle dependent on the torque and is in contrast

Manuscript received June 15, 2016; revised December 17, 2016; accepted March 15, 2017. Manuscript received in final form March 28, 2017. Recommended by Associate Editor A. Chiuso. This work was supported in part by the University of Macau under Project MYRG2015-00127-FST and Project MYRG2015-00126-FST and in part by the Fundação para a Ciência e a Tecnologia through ISR under Grant LARSyS UID/EEA/50009/2013 and through IDMEC under Grant LAETA Pest-OE/EME/LA0022. *(Corresponding author: David Cabecinhas.)*

D. Cabecinhas is with the Department of Electrical and Computer Engineering, Faculty of Science and Technology, of the University of Macau, Macao 999078, China. He is also with the Institute for Systems and Robotics, LARSyS, Portugal (e-mail: dcabecinhas@umac.mo).

P. Batista is with the Department of Electrical and Computer Engineering and also with the Institute for Systems and Robotics, Instituto Superior Técnico, Universidade de Lisboa, Lisboa 1049-001, Portugal (e-mail: pbatista@isr.tecnico.ulisboa.pt).

P. Oliveira is with the Associated Laboratory for Energy, Transports and Aeronautics, Institute of Mechanical Engineering and the collaborator of ISR/LARSyS, both at Instituto Superior Técnico, Universidade de Lisboa, Lisbon 1049-001, Portugal (e-mail: pjcro@isr.tecnico.ulisboa.pt).

C. Silvestre is with the Department of Electrical and Computer Engineering of the Faculty of Science and Technology of the University of Macau, Macao 999078, China, on leave from the Instituto Superior Técnico/Universidade de Lisboa, Lisboa 1049-001, Portugal (e-mail: csilvestre@umac.mo).

Color versions of one or more of the figures in this paper are available online at http://ieeexplore.ieee.org.

Digital Object Identifier 10.1109/TCST.2017.2692733

1063-6536 © 2017 IEEE. Personal use is permitted, but republication/redistribution requires IEEE permission.
See http://www.ieee.org/publications_standards/publications/rights/index.html for more information.

This article has been accepted for inclusion in a future issue of this journal. Content is final as presented, with the exception of pagination.

with the model used on the above-mentioned works, wherein hovercraft are driven by two propellers and thrust and torque are independent. Additionally, an online estimation algorithm continuously estimates the drag parameters of the hovercraft, thus allowing for improved performance over different scenarios, and the stability of the overall closed-loop system is analyzed.

This paper is structured as follows. Section II presents a formal statement for the trajectory tracking control and parameter estimation problems. The general framework for identification of the unknown parameters is outlined in Section III. The hovercraft model is specified in Section IV, followed by the particularization of the parameter estimator design to the hovercraft model in Section V. The controller design procedure is described in detail in Section VI and its closed-loop interconnection with the parameter estimator is analyzed in Section VII. Simulation and experimental results that attest the performance and stability of the proposed parameter estimator and trajectory tracking controller are presented in Section VIII followed by the conclusions in Section IX.

II. Problem Statement

The problems tackled in this paper are threefold and culminate in a coherent integrated solution. We propose to estimate constant parameters for a broad dynamic model category, to design a nonlinear controller for a particular nonlinear dynamic model in that category, and finally, to analyze the stability of the closed-loop interconnection between the estimator and the controller.

A generic nonlinear dynamic system can be represented by the differential equation system

$$\dot{\mathbf{x}} = \mathbf{h}_0(\mathbf{x}, \boldsymbol{\zeta}, t)$$

where $\mathbf{x} \in \mathbb{R}^n$ represents the state of the dynamical system, $\boldsymbol{\zeta} \in \mathbb{R}^m$ represents unknown parameters of the system, and $\mathbf{h}_0(\mathbf{x}, \boldsymbol{\zeta}, t) : \mathbb{R}^n \times \mathbb{R}^m \times \mathbb{R} \to \mathbb{R}^n$. In this paper, we focus on nonlinear systems that are linear-in-parameters, i.e., dynamical systems that can be represented by the state dynamics

$$\dot{\mathbf{x}} = \mathbf{h}(\mathbf{x}, t) + \mathbf{G}(\mathbf{x}, t)\boldsymbol{\zeta} \tag{1}$$

with $\mathbf{h}(\mathbf{x}, t) : \mathbb{R}^n \times \mathbb{R} \to \mathbb{R}^n$ and $\mathbf{G}(\mathbf{x}, t) : \mathbb{R}^n \times \mathbb{R} \to \mathbb{R}^{n \times m}$.

The estimation problem tackled in this paper consists in designing an exponentially stable estimator for the unknown parameters $\boldsymbol{\zeta}$ for a dynamic system with structure (1) of which full state measurements are available.

As a particular example of a dynamic system with structure (1) we consider a hovercraft, an underactuated dynamic system, where the parameters are the drag and input coefficients. The control objective is to design a state feedback controller for the hovercraft's inputs, thrust force, and rudder angle, with the objective of tracking a predefined trajectory.

The final objective is to prove that the closed-loop interconnection of the parameter estimator, particularized for the hovercraft dynamics, and the tracking controller is stable under mild assumptions on the initial conditions. This is a strong result on the interconnection of two nonlinear dynamic systems, which is much more challenging to analyze than the interconnection of two linear systems.

III. Identification Framework

Using state augmentation with the unknown parameters, the previous dynamical system can be written in block form as

$$\begin{bmatrix} \dot{\mathbf{x}} \\ \dot{\boldsymbol{\zeta}} \end{bmatrix} = \begin{bmatrix} \mathbf{0} & \mathbf{G}(\mathbf{x}, t) \\ \mathbf{0} & \mathbf{0} \end{bmatrix} \begin{bmatrix} \mathbf{x} \\ \boldsymbol{\zeta} \end{bmatrix} + \begin{bmatrix} \mathbf{h}(\mathbf{x}, t) \\ \mathbf{0} \end{bmatrix}. \tag{2}$$

Assuming that full state measurements are available, we have

$$\mathbf{y} = [\mathbf{I} \quad \mathbf{0}] \begin{bmatrix} \mathbf{x} \\ \boldsymbol{\zeta} \end{bmatrix} \tag{3}$$

where the explicit dependence of $\mathbf{x}$, $\boldsymbol{\zeta}$, and $\mathbf{y}$ on the time t is omitted for the sake of simplicity.

The nonlinear system linear-in-the-parameters comprising the state (2) and output (3) can thus be rewritten as a linear time-varying (LTV) system

$$\begin{cases} \dot{\boldsymbol{\xi}} = \mathbf{A}(t)\boldsymbol{\xi} + \mathbf{u}(t) \\ \mathbf{y} = \mathbf{C}(t)\boldsymbol{\xi} \end{cases} \tag{4}$$

with

$$\begin{aligned} \mathbf{A}(t) &= \begin{bmatrix} \mathbf{0} & \mathbf{G}(\mathbf{y}, t) \\ \mathbf{0} & \mathbf{0} \end{bmatrix}, \quad \mathbf{u}(t) = \begin{bmatrix} \mathbf{h}(\mathbf{y}, t) \\ \mathbf{0} \end{bmatrix} \\ \mathbf{C}(t) &= [\mathbf{I} \quad \mathbf{0}], \quad \boldsymbol{\xi} = \begin{bmatrix} \mathbf{x} \\ \boldsymbol{\zeta} \end{bmatrix}. \end{aligned} \tag{5}$$

Notice that, where appropriate, $\mathbf{x}$ was replaced by $\mathbf{y}$ so that the system can be regarded as linear, as $\mathbf{y}$ is available for estimator design purposes. We now introduce the following Lemma [7] regarding the observability of system (4):

Lemma 1: Consider the nonlinear system (4). If the observability Grammian $\mathbf{W}(t_0, t_f)$ associated with the pair $(\mathbf{A}(t), \mathbf{C}(t))$ on $\mathcal{I} = [t_0, t_f]$ is invertible then the nonlinear system (4) is observable in the sense that, given the system input $\{\mathbf{u}(t), t \in \mathcal{I}\}$ and the system output $\{\mathbf{y}(t), t \in \mathcal{I}\}$, the initial condition $\boldsymbol{\xi}(t_0)$ is uniquely defined.

Given the system input $\mathbf{u}(t), t \in \mathcal{I}$, and the system output $\mathbf{y}(t), t \in \mathcal{I}$, it is possible to compute the transition matrix associated with $\mathbf{A}(t)$ through the Peano–Baker series as

$$\begin{aligned} \boldsymbol{\Phi}(t, t_0) = \mathbf{I} &+ \int_{t_0}^{t_f} \mathbf{A}(\sigma_1) d\sigma_1 \\ &+ \int_{t_0}^{t_f} \mathbf{A}(\sigma_1) \int_{t_0}^{\sigma_1} \mathbf{A}(\sigma_2) d\sigma_2 d\sigma_1 \\ &+ \int_{t_0}^{t_f} \mathbf{A}(\sigma_1) \int_{t_0}^{\sigma_1} \mathbf{A}(\sigma_2) \int_{t_0}^{\sigma_2} \mathbf{A}(\sigma_3) d\sigma_3 d\sigma_2 d\sigma_1 \ldots \end{aligned}$$

The block structure of $\mathbf{A}(t)$ in (5) can be explored to simplify the transition matrix by noting that $\mathbf{A}(t)$ is nilpotent, with $\mathbf{A}^n(t) = \mathbf{0}$ for $n \geq 2$. This reduces the transition matrix to

$$\boldsymbol{\Phi}(t, t_0) = \mathbf{I} + \int_{t_0}^{t_f} \mathbf{A}(\sigma) d\sigma = \begin{bmatrix} \mathbf{I} & \int_{t_0}^{t_f} \mathbf{G}(\mathbf{y}, \sigma) d\sigma \\ \mathbf{0} & \mathbf{I} \end{bmatrix}.$$

This article has been accepted for inclusion in a future issue of this journal. Content is final as presented, with the exception of pagination.

The observability Grammian is then given as

$$\begin{aligned}\mathbf{W}(t_0,t_f) &= \int_{t_0}^{t_f} \mathbf{\Phi}^T(t,t_0)\mathbf{C}^T(t)\mathbf{C}(t)\mathbf{\Phi}(t,t_0)dt \\ &= \int_{t_0}^{t_f} \left[\int_{t_0}^{t_f} \begin{matrix}\mathbf{I} \\ \mathbf{G}^T(\mathbf{y},\sigma)d\sigma\end{matrix}\right]\left[\mathbf{I}\int_{t_0}^{t_f}\mathbf{G}(\mathbf{y},\sigma)d\sigma\right]dt.\end{aligned} \tag{6}$$

The structure of $\mathbf{A}(t)$ can be used to derive further conditions on the invertibility of the Grammian $\mathbf{W}(t_0,t_f)$, as stated in Lemma 2.

Lemma 2: Consider the nonlinear system (4) with realization (5), corresponding to a general nonlinear system with linear unknown parameters. If there exists no unit vector $\mathbf{d}\in\mathbb{R}^m$ that satisfies the condition

$$\int_{t_0}^{t}\mathbf{G}(\mathbf{y},\sigma)d\sigma\,\mathbf{d}=\mathbf{0}$$

for all time $t\in\mathcal{I}$ then the nonlinear system (4) is observable in the sense that, given the system input $\{\mathbf{u}(t), t\in\mathcal{I}\}$ and the system output $\{\mathbf{y}(t), t\in\mathcal{I}\}$, the initial condition $\boldsymbol{\xi}(t_0)$ is uniquely defined.

Proof: From Lemma 1 we have that the observability of the nonlinear system depends on the invertibility of the Grammian (6). Due to its symmetric nature, it has nonnegative eigenvalues and is invertible if and only if it is positive definite. To explore the definite-positiveness conditions for $\mathbf{W}(t_0,t_f)$ we introduce $\mathbf{d}\in\mathbb{R}^{n+m}$ as a unit vector and consider

$$\begin{aligned}&\mathbf{d}^T\mathbf{W}(t_0,t_f)\mathbf{d} \\ &= \mathbf{d}^T\int_{t_0}^{t_f}\left[\int_{t_0}^{t_f}\begin{matrix}\mathbf{I}\\ \mathbf{G}^T(\mathbf{y},\sigma)\end{matrix}\right]\left(\left[\mathbf{I}\int_{t_0}^{t}\mathbf{G}(\mathbf{y},\sigma)d\sigma\right]\right)dt\mathbf{d} \\ &= \int_{t_0}^{t_f}\left\|\left[\mathbf{I}\int_{t_0}^{t}\mathbf{G}(\mathbf{y},\sigma)d\sigma\right]\mathbf{d}\right\|^2 dt.\end{aligned}$$

The proof follows by contraposition. Suppose that the system is not observable. Then, from Lemma 1, the observability Grammian $\mathbf{W}(t_0,t_f)$ associated with the pair $(\mathbf{A}(t),\mathbf{C}(t))$ is not positive definite. Hence, there exists $\mathbf{d}\in\mathbb{R}^{n+m}$, $\|\mathbf{d}\|=1$, such that $\mathbf{d}^T\mathbf{W}(t_0,t_f)\mathbf{d}=0$, or equivalently

$$\int_{t_0}^{t_f}\left\|\left[\mathbf{I}\int_{t_0}^{t}\mathbf{G}(\mathbf{y},\sigma)d\sigma\right]\mathbf{d}\right\|^2 dt=0.$$

As the integrand is nonnegative the previous equation implies

$$\left[\mathbf{I}\int_{t_0}^{t}\mathbf{G}(\mathbf{y},\sigma)d\sigma\right]\mathbf{d}=\mathbf{0}$$

for all time $t\in\mathcal{I}$. Let us partition the unit vector as $\mathbf{d}=\begin{bmatrix}\mathbf{d}_1 & \mathbf{d}_2\end{bmatrix}$ with $\mathbf{d}_1\in\mathbb{R}^n$ and $\mathbf{d}_2\in\mathbb{R}^m$. The nonobservability condition can then be written as

$$\mathbf{d}_1+\int_{t_0}^{t}\mathbf{G}(\mathbf{y},\sigma)d\sigma\,\mathbf{d}_2=0$$

which must be verified for all time for the LTV system to be nonobservable. In particular, it must be observed for $t=t_0$, which leads immediately to conclude $\mathbf{d}_1=0$. But as $\mathbf{d}$ is a unit vector, it then follows that, if the system is not observable, there must exist a unit vector $\mathbf{d}_2$ such that

$$\int_{t_0}^{t}\mathbf{G}(\mathbf{y},\sigma)d\sigma\,\mathbf{d}_2=\mathbf{0} \tag{7}$$

for all time $t\in\mathcal{I}$, which concludes the proof by contraposition. □

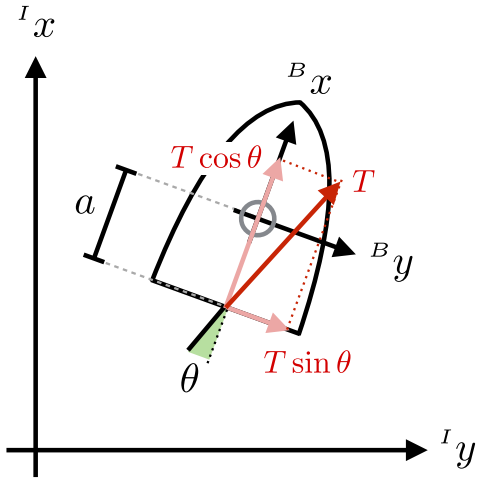

Fig. 1. Sketch of hovercraft model.

In the following section, we present the dynamic model for the hovercraft. The general conditions for estimator design outlined in this section will be particularized for the hovercraft in Section V, where concrete observability conditions are outlined.

IV. Hovercraft Model

The hovercraft, depicted in Fig. 1, is modeled as a rigid body in a 2-D space. Defining the *body frame* $\{B\}$ as a reference frame attached to the hovercraft's center of mass and $\{I\}$ as an *inertial frame*, and omitting the explicit time dependence, we have the following kinematics and dynamics for the hovercraft:

$$\begin{cases}\dot{\mathbf{p}}=\mathbf{R}\mathbf{v}\\ \dot{\mathbf{R}}=\mathbf{R}\mathbf{S}r\\ m\dot{\mathbf{v}}=-m\mathbf{S}\mathbf{v}r+\mathbf{f}\\ J\dot{r}=\tau\end{cases} \tag{8}$$

where $\mathbf{p}\in\mathbb{R}^2$ is the hovercraft's position in $\{I\}$, $\mathbf{v}=[u\ v]^T\in\mathbb{R}^2$ is the velocity expressed in $\{B\}$, $r\in\mathbb{R}$ is the angular velocity, $\mathbf{R}\in\mathrm{SO}(2)$ is the rotation matrix that takes vectors expressed in $\{B\}$ to $\{I\}$, and $\mathbf{f}$ and τ are the total force and torque acting on the vehicle, respectively. The mass is $m>0$, the inertia $J>0$, and the auxiliary skew-symmetric matrix is

$$\mathbf{S}=\begin{bmatrix}0 & -1\\ 1 & 0\end{bmatrix}.$$

The forces acting on the hovercraft comprise the thrust force actuation as well as the aerodynamic and friction drag. The thrust force generated by the propeller is divided between surge and sway forces by the rudder, with the sway force also generating a torque around the center of mass. In the hovercraft setup the angle and thrust force are known but the

This article has been accepted for inclusion in a future issue of this journal. Content is final as presented, with the exception of pagination.

coefficients multiplying each term are not. Given the nature of the drag we consider two components: one independent of the velocity (dry friction, friction with the ground) and one linear with the velocity (laminar flow friction). The drag coefficient multiplying the velocities, as well as the dry friction coefficient, are unknown and must be estimated. This leads to the following expressions for the force and torque:

$$\mathbf{f} = \begin{bmatrix} -d_{u0}\operatorname{sign} u - d_u u + b_T T\cos\theta \\ -d_{v0}\operatorname{sign} v - d_v v + b_T T\sin\theta \end{bmatrix} \tag{9}$$

$$\tau = -d_{r0}\operatorname{sign} r - d_r r - a b_T T\sin\theta \tag{10}$$

where $\{d_{u0}, d_u, d_{v0}, d_v, d_{r0}, d_r, b_T\} \in \mathbb{R}$ are the unknown coefficients corresponding to the friction coefficients (d_{u0}, d_{v0}, d_{r0}), linear drag coefficients (d_u, d_v, d_r), and input scaling coefficient b_T. The length of the arm from the center of mass to the rudder surface is denoted by a, as evidenced in Fig. 1, T is the thrust force, and θ corresponds to the rudder angle. The coefficient b_T scales the thrust input from $[0, 1]$ (range of remote control input) to force in Newtons and makes unnecessary an *a priori* thrust identification. Indeed, with the proposed approach the identification of the dynamic system can be performed without having to determine the exact force generated by the thrust propeller, in Newton.

Particularizing the general hovercraft dynamics with (9) and (10) we get the explicit dynamics

$$\begin{cases} \dot{u} = -m^{-1}d_{u0}\operatorname{sign} u - m^{-1}d_u u + m^{-1}b_T T\cos\theta + vr \\ \dot{v} = -m^{-1}d_{v0}\operatorname{sign} v - m^{-1}d_v v + m^{-1}b_T T\sin\theta - ur \\ \dot{r} = -J^{-1}d_{r0}\operatorname{sign} r - J^{-1}d_r r - J^{-1}a b_T T\sin\theta. \end{cases} \tag{11}$$

V. Parameter Estimator Design

The linear structure of the unknown parameters can be exploited to rewrite the hovercraft system in LTV form explicitly, which will prove instrumental in designing an estimator for the unknown parameters. Focusing on the dynamics, a system where the velocities are measured and the parameters are unknown can be written in LTV form as (4) with realization

$$\begin{aligned} \mathbf{x} &= [u \quad v \quad r]^T \\ \boldsymbol{\zeta} &= [m^{-1}d_{u0} \quad m^{-1}d_u \quad m^{-1}d_{v0} \quad m^{-1}d_v \quad J^{-1}d_{r0} \quad J^{-1}d_r \\ &\qquad m^{-1}b_T \quad J^{-1}ab_T]^T \end{aligned} \tag{12}$$

$$\mathbf{A}(t) = \begin{bmatrix} \mathbf{0}_{3\times3} & \mathbf{G}(\mathbf{y},t) \\ \mathbf{0}_{8\times3} & \mathbf{0}_{8\times8} \end{bmatrix}, \quad \mathbf{u}(t) = \begin{bmatrix} vr \\ -ur \\ 0 \\ \mathbf{0}_{8\times1} \end{bmatrix}$$

$$\mathbf{C}(t) = \begin{bmatrix} \mathbf{I}_{3\times3} & \mathbf{0}_{3\times8} \end{bmatrix} \tag{13}$$

where the auxiliary matrix $\mathbf{G}(\mathbf{y}, t)$ is

$$\mathbf{G}(\mathbf{y},t) = [\mathbf{G}_u(\mathbf{y},t) \quad \mathbf{G}_v(\mathbf{y},t) \quad \mathbf{G}_r(\mathbf{y},t) \quad \mathbf{G}_T(\mathbf{y},t)]$$

with

$$\mathbf{G}_u(\mathbf{y},t) = \begin{bmatrix} -\operatorname{sign} u(t) & -u(t) \\ 0 & 0 \\ 0 & 0 \end{bmatrix}$$

$$\mathbf{G}_v(\mathbf{y},t) = \begin{bmatrix} 0 & 0 \\ -\operatorname{sign} v(t) & -v(t) \\ 0 & 0 \end{bmatrix}$$

$$\mathbf{G}_r(\mathbf{y},t) = \begin{bmatrix} 0 & 0 \\ 0 & 0 \\ -\operatorname{sign} r(t) & -r(t) \end{bmatrix}$$

$$\mathbf{G}_T(\mathbf{y},t) = \begin{bmatrix} T(t)\cos\theta(t) & 0 \\ T(t)\sin\theta(t) & 0 \\ 0 & -T(t)\sin\theta(t) \end{bmatrix}.$$

Starting with the nonobservability condition (7) particularized for the hovercraft dynamics and taking time derivatives on both sides we get the equivalent nonobservability condition of

$$\begin{cases} -\operatorname{sign} u(t)d_{21} - u(t)d_{22} + T(t)\cos\theta(t)d_{27} = 0 \\ -\operatorname{sign} v(t)d_{23} - v(t)d_{24} + T(t)\sin\theta(t)d_{27} = 0 \\ -\operatorname{sign} r(t)d_{25} - r(t)d_{26} - T(t)\sin\theta(t)d_{28} = 0 \end{cases}$$

for all $t \in \mathcal{I}$, where d_{2i}, for $i = \{1, \cdots, 8\}$, are the components of the unit vector $\mathbf{d}_2$ in (7).

The system (4) with realization (13) is observable if and only if the sets of functions

$$\{\operatorname{sign} u(t),\ u(t),\ T(t)\cos(\theta(t))\} \tag{14a}$$

$$\{\operatorname{sign} v(t),\ v(t),\ T(t)\sin(\theta(t))\} \tag{14b}$$

$$\{\operatorname{sign} r(t),\ r(t),\ T(t)\sin(\theta(t))\} \tag{14c}$$

are linearly independent in $\mathcal{I}$. Simply put, as long as the actuations $T(t)$ and $\theta(t)$ are not constant and sufficiently rich, then the LTV system is observable and we can recover the unknown system parameters. Given the LTV structure, a Kalman filter provides a simple and easily tunable solution. In the event some of the sets of functions (14a), (14b), and (14c) are not linearly independent, the stability of the estimator system is still ensured and estimates converge to a constant, although they are not guaranteed to converge to the correct parameters.

To conclude this section notice that stronger forms of observability should be imposed for the stability of the Kalman filter. In particular, if the LTV system (4) is uniformly complete observable, then the Kalman filter is globally exponentially stable [8], [9]. This form of observability is closely related to the one previously derived, but further imposes that the linear independence of the functions in (14a), (14b), and (14c) must happen uniformly throughout all time and that each individual function must not degenerate into another.

VI. Controller Design

The controller objective is to have a fixed point $\boldsymbol{\delta} \in \mathbb{R}^2$ in the body frame, not necessarily the center of mass, to track a desired trajectory $\mathbf{p}_d$, where in the following the explicit time dependence will be neglected for the sake of simplicity. The tracking error is defined in the inertial frame as

$$\mathbf{z}_1 = \mathbf{p} - \mathbf{p}_d + \mathbf{R}\boldsymbol{\delta} \tag{15}$$

and we denote its time derivative by

$$\mathbf{z}_2 = \dot{\mathbf{z}}_1 = \mathbf{R}\mathbf{v} - \dot{\mathbf{p}}_d + \mathbf{R}\mathbf{S}\boldsymbol{\delta} r. \tag{16}$$

This article has been accepted for inclusion in a future issue of this journal. Content is final as presented, with the exception of pagination.

The second time derivative of the tracking error is

$$\begin{aligned}\dot{\mathbf{z}}_2 &= \ddot{\mathbf{z}}_1 \\ &= \mathbf{RSv}r + m^{-1} \\ &\quad \cdot R\left(-m\mathbf{Sv}r + \begin{bmatrix} -d_{u0}\operatorname{sign} u - d_u u + b_T T\cos\theta \\ -d_{v0}\operatorname{sign} v - d_v v + b_T T\sin\theta \end{bmatrix}\right) \\ &\quad - \ddot{\mathbf{p}}_d + \mathbf{RS}^2\boldsymbol{\delta}r^2 + \mathbf{RS}\boldsymbol{\delta}J^{-1} \\ &\quad \cdot(-d_{r0}\operatorname{sign} r - d_r r - ab_T T\sin\theta)\end{aligned}$$

and can be seen as the input, where T and θ are arbitrary signals, for a double integrator whose output is the tracking error. The proposed controller can accommodate arbitrary vectors $\boldsymbol{\delta}$ for the point in the body-fixed frame to be controlled. However, in order to preserve the symmetry of the vehicle we assume throughout the remainder of this paper that the point is of the form

$$\boldsymbol{\delta} = \begin{bmatrix} \delta_x \\ 0 \end{bmatrix}$$

with $\delta_x \in \mathbb{R}$.

The proposed controller is designed based on Lyapunov theory and uses the double integrator structure of the tracking error system as a departure point. We now apply a typical Lyapunov function for a double integrator

$$V = \frac{1}{2}k_1\mathbf{z}_1^T\mathbf{z}_1 + \frac{1}{2}\mathbf{z}_2^T\mathbf{z}_2 + \beta\mathbf{z}_1^T\mathbf{z}_2 \tag{17}$$

to the error system with $k_1 > 0$ and $\beta > 0$. Its time derivative can be written as

$$\dot{V} = -W(\mathbf{z}_1, \mathbf{z}_2) + (\beta\mathbf{z}_1 + \mathbf{z}_2)^T(\dot{\mathbf{z}}_2 + k_1\mathbf{z}_1 + k_2\mathbf{z}_2)$$

where

$$W(\mathbf{z}_1, \mathbf{z}_2) = k_1\beta\mathbf{z}_1^T\mathbf{z}_1 + k_2\beta\mathbf{z}_1^T\mathbf{z}_2 + (k_2 - \beta)\mathbf{z}_2^T\mathbf{z}_2$$

with $k_2 > 0$. In order for $V(\mathbf{z}_1, \mathbf{z}_2)$ and $W(\mathbf{z}_1, \mathbf{z}_2)$ to be definite positive functions the coefficient β is required to observe

$$\beta < \sqrt{k_1} \tag{18}$$

$$\beta < \frac{4k_1k_2}{4k_1 + k_2^2}. \tag{19}$$

Expanding $\dot{\mathbf{z}}_2$ and grouping the actuations T and θ one gets

$$\begin{aligned}\dot{V} &= -W(\mathbf{z}_1, \mathbf{z}_2) + (\beta\mathbf{z}_1 + \mathbf{z}_2)^T\mathbf{R} \\ &\quad \cdot\left(\mathbf{B}T\begin{bmatrix}\cos\theta \\ \sin\theta\end{bmatrix} + m^{-1}\begin{bmatrix} -d_{u0}\operatorname{sign} u - d_u u \\ -d_{v0}\operatorname{sign} v - d_v v\end{bmatrix}\right. \\ &\qquad - \mathbf{R}^T\ddot{\mathbf{p}}_d - \delta_x r^2\mathbf{e}_1 - J^{-1}(d_{r0}\operatorname{sign} r + d_r r)\delta_x\mathbf{e}_2 \\ &\qquad \left. + \mathbf{R}^T(k_1\mathbf{z}_1 + k_2\mathbf{z}_2)\right)\end{aligned} \tag{20}$$

with the auxiliary matrix

$$\mathbf{B} = b_T\begin{bmatrix} m^{-1} & 0 \\ 0 & m^{-1} - J^{-1}\delta_x a\end{bmatrix} \tag{21}$$

and unit vectors $\mathbf{e}_1 = [1\ 0]^T$ and $\mathbf{e}_2 = [0\ 1]^T$.

The fact that both actuations T and θ appear in the Lyapunov derivative (20) and span $\mathbb{R}^2$ allows us to state the following theorem, where a stabilizing controller is proposed for the tracking error system.

Theorem 3: Let the hovercraft dynamics be described by (8) with external force (9) and external torque (10) and consider the system states (15) and (16), where $\boldsymbol{\delta} = [\delta_x\ 0]^T$ is a fixed point on the body frame and $\mathbf{p}_d$ is a bounded reference trajectory with bounded time derivatives. Choosing the arm length a and δ_x such that (21) is invertible, that is

$$a\delta_x \neq m^{-1}J$$

and applying the control actions for thrust T and rudder angle θ such that

$$\begin{aligned}T\begin{bmatrix}\cos\theta \\ \sin\theta\end{bmatrix} &= -\mathbf{B}^{-1}\left(m^{-1}\begin{bmatrix} -d_{u0}\operatorname{sign} u - d_u u \\ -d_{v0}\operatorname{sign} v - d_v v\end{bmatrix} - \mathbf{R}^T\ddot{\mathbf{p}}_d\right. \\ &\quad - \delta_x r^2\mathbf{e}_1 - J^{-1}(d_{r0}\operatorname{sign} r + d_r r)\delta_x\mathbf{e}_2 \\ &\quad \left. + \mathbf{R}^T(k_1\mathbf{z}_1 + k_2\mathbf{z}_2)\right)\end{aligned} \tag{22}$$

with $k_1 > 0$ and $k_2 > 0$, renders the origin of the dynamic system globally exponentially stable.

Proof: With the imposed restrictions in k_1, k_2, and β verifying (18) and (19), the Lyapunov function (17) is positive definite and radially unbounded. Using the control law (22) to define the system actuation, the closed-loop time derivative of the aforementioned function is rendered definite negative

$$\dot{V} = -W(\mathbf{z}_1, \mathbf{z}_2).$$

From Lyapunov's stability theorems it follows that the origin of the error system is globally exponentially stable. □

The individual actuations T and θ are recovered noting that for $a, b \in \mathbb{R}$ and

$$T\begin{bmatrix}\cos\theta \\ \sin\theta\end{bmatrix} = \begin{bmatrix} a \\ b\end{bmatrix}$$

we have

$$\begin{aligned}T &= \|[a\quad b]\| \\ \theta &= \operatorname{atan2}(b, a)\end{aligned}$$

where $\operatorname{atan2}(y, x)$ is the four-quadrant inverse tangent that returns the angle of the vector (x, y) respecting its quadrant.

From the exponential stability of the tracking errors it follows that the tracking errors $\mathbf{z}_1$ and $\mathbf{z}_2$ converge to zero and trajectory tracking is achieved.

Notice that Theorem 3 does not prescribe any conditions on a or δ_x except for $a\delta_x \neq m^{-1}J$. This means that neither δ_x nor a has a restriction on their signs. However, negative δ_x or a can lead to nondesirable transients and steady-state modes for the hovercraft system and lead to conditions on which the dynamic model (8) ceases to be valid, such as leading the hovercraft to follow the trajectory with its stern facing the direction of movement.

A. Analysis of the Zero Dynamics

The proposed trajectory tracking controller in Theorem 3 ensures that the errors $\mathbf{z}_1$ and $\mathbf{z}_2$ converge to zero. However, to conclude about the internal stability of the dynamic system we must analyze its zero dynamics and ensure that inner

This article has been accepted for inclusion in a future issue of this journal. Content is final as presented, with the exception of pagination.

states such as the linear and angular velocities do not grow unbounded.

We proceed to analyze the dynamic evolution of the velocities by considering the angular kinetic energy of the system

$$Z = \frac{1}{2} r^2.$$

Substituting $\dot{r}$ for the explicit dynamics (11) with the closed-loop control law (22) results in the following closed-loop time derivative for the angular kinetic energy

$$\begin{aligned}\dot{Z} = r J^{-1}(&-d_{r0} \operatorname{sign} r - d_r r + a\ (m^{-1} - J^{-1}\delta_x a)^{-1} \\ &\cdot\ (m^{-1}(-d_{v0} \operatorname{sign} v - d_v v) \\ &-\ J^{-1}(d_{r0} \operatorname{sign} r + d_r r)\delta_x \\ &+\ \mathbf{e}_2^T \mathbf{R}^T\ (k_1 \mathbf{z}_1 + k_2 \mathbf{z}_2 - \ddot{\mathbf{p}}_d))).\end{aligned}$$

From the definition of $\mathbf{z}_2$ in (16) and recalling that $\boldsymbol{\delta} = \delta_x \mathbf{e}_1$ we have the relation

$$v = \mathbf{e}_2^T R^T (\mathbf{z}_2 + \dot{\mathbf{p}}_d) - \delta_x r.$$

Substituting the sway velocity v into the energy derivative one gets

$$\begin{aligned}\dot{Z} = r J^{-1}\big(&-d_{r0} \operatorname{sign} r - d_r r + a\ (m^{-1} - J^{-1}\delta_x a)^{-1} \\ &\cdot \big(m^{-1}\big(-d_{v0} \operatorname{sign} \mathbf{e}_2^T R^T (\mathbf{z}_2 + \dot{\mathbf{p}}_d) - \delta_x r \\ &\qquad - d_v\big(\mathbf{e}_2^T R^T \big(\mathbf{z}_2 + \dot{\mathbf{p}}_d\big) - \delta_x r\big)\big) \\ &-\ J^{-1}(d_{r0} \operatorname{sign} r + d_r r)\delta_x \\ &+\ \mathbf{e}_2 \mathbf{R}^T\ (k_1 \mathbf{z}_1 + k_2 \mathbf{z}_2 - \ddot{\mathbf{p}}_d)\big)\big).\end{aligned}$$

Further simplifications and gathering all terms with r^2 at the beginning leads to the final expression

$$\begin{aligned}\dot{Z} = &-J^{-1} d_{r0} \operatorname{sign} r r + [-J^{-1} d_r + J^{-1} a (m^{-1} - J^{-1}\delta_x a)^{-1} \\ &\qquad \times\ (m^{-1} d_v - J^{-1} d_r)\delta_x] r^2 \\ &+ r J^{-1}\big(a(m^{-1} - J^{-1}\delta_x a)^{-1} \\ &\qquad \cdot\ \big(m^{-1}\big(-d_{v0} \operatorname{sign} \mathbf{e}_2^T R^T \big(\mathbf{z}_2 + \dot{\mathbf{p}}_d\big) - \delta_x r \\ &\qquad -\ d_v \mathbf{e}_2^T R^T (\mathbf{z}_2 + \dot{\mathbf{p}}_d)\big) - J^{-1} d_{r0} \operatorname{sign} r \delta_x \\ &\qquad +\ \mathbf{e}_2 \mathbf{R}^T (k_1 \mathbf{z}_1 + k_2 \mathbf{z}_2 - \ddot{\mathbf{p}}_d))\big). \qquad (23)\end{aligned}$$

At this point, we are able to state a formal result on the stability of the zero dynamics of the closed-loop system. Theorem 4 states conditions for which it can be shown that escape to infinity of the velocities is impossible.

Theorem 4: Consider the hovercraft dynamics (8) in closed loop with the trajectory tracking controller (22). For any arm length a of the vehicle there exists a constant $\Delta > 0$ such that if the control point satisfies $\|\delta_x\| < \Delta$ and $a\delta_x \neq m^{-1} J$, then the linear velocity $\mathbf{v} = [u\ v]^T$ and angular velocity r of the vehicle are bounded.

Proof: From Theorem 3, it follows that the tracking errors $\mathbf{z}_1$ and $\mathbf{z}_2$ are bounded and so are the parameters gathered in $\boldsymbol{\zeta}$, the mass and inertia moment, as well as the reference trajectory and its derivatives. For large velocities, the time derivative of the angular kinetic energy Z, expressed in (23), is dominated by the term in r^2, given that all the other terms are bounded and multiply r linearly. We can thus conclude from (23) that boundedness of r is achieved if the condition

$$J^{-1} d_r > \delta_x a (m^{-1} - J^{-1}\delta_x a)^{-1}(m^{-1} d_v - J^{-1} d_r) \qquad (24)$$

is verified. This condition can always be satisfied either by choosing a small enough rudder arm length a (at the vehicle design phase) or a sufficiently small control point distance δ_x (at the controller design phase). From the definition of the tracking error $\mathbf{z}_2$ and boundedness of $\mathbf{z}_2$ and r it follows also that the linear velocities u and v are also bounded. □

It should be noticed that the product

$$a\delta_x\ (m^{-1} - J^{-1} a \delta_x)^{-1}$$

goes to zero as either a or δ_x goes to zero. This allows the right-hand side of (24) to be arbitrarily close to zero, choosing suitable a and δ_x, and to verify (24) since J and d_r are positive.

VII. Interconnection Stability Analysis

The control law (22) can be expressed in terms of the parameters (12) as

$$\begin{aligned}T \begin{bmatrix}\cos\theta \\ \sin\theta\end{bmatrix} = -\mathbf{B}^{-1} \Bigg(&-\begin{bmatrix}\zeta_1 \operatorname{sign} u + \zeta_2 u \\ \zeta_3 \operatorname{sign} v + \zeta_4 v\end{bmatrix} \\ &-\ (\zeta_5 \operatorname{sign} r + \zeta_6 r)\delta_x \mathbf{e}_2 \\ &-\ \mathbf{R}^T \ddot{\mathbf{p}}_d - \delta_x r^2 \mathbf{e}_1 \\ &+\ \mathbf{R}^T (k_1 \mathbf{z}_1 + k_2 \mathbf{z}_2)\Bigg) \qquad (25)\end{aligned}$$

with $\mathbf{B}$, defined in (21), also rewritten in terms of (12) as

$$\mathbf{B} = \begin{bmatrix}\zeta_7 & 0 \\ 0 & \zeta_7 - \zeta_8 \delta_x\end{bmatrix}. \qquad (26)$$

To study the overall closed-loop system that results from the proposed controller and proposed parameter estimator we start by determining the actuation error, obtained using the estimate $\hat{\boldsymbol{\zeta}}$ for the parameters $\boldsymbol{\zeta}$, with regard to the ideal feedback actuation. The error is given by

$$T \begin{bmatrix}\cos\theta \\ \sin\theta\end{bmatrix} - \hat{T} \begin{bmatrix}\cos\hat{\theta} \\ \sin\hat{\theta}\end{bmatrix}$$

where the hat terms are obtained using (25) and (26) with the estimates $\hat{\boldsymbol{\xi}}$ instead of the real parameters $\boldsymbol{\xi}$.

During a normal run of the hovercraft the only parameters that are expected to change are the ones related to friction, ζ_1 to ζ_6, which can depend on the terrain. The actuation parameters are well-determined *a priori* and do not change during the experimental run. The closed-loop Lyapunov function time derivative resulting from the mismatch between the estimated and real parameters is then given as

where we used $\tilde{\boldsymbol{\zeta}} = \boldsymbol{\zeta} - \hat{\boldsymbol{\zeta}}$ for the parameter error. Making use of Theorems 3 and 4 we can summarize the closed-loop interconnection stability analysis as follows.

Theorem 5: Consider a hovercraft with dynamics (8) in closed loop with the control law (22) and with online estimation of the drag related parameters ζ_1 to ζ_6 from (12) such that the control point $\boldsymbol{\delta} = [\delta_x\ 0]^T$ satisfies the conditions of Theorem 4 for stable zero dynamics. In these circumstances, if the functions (14a)-(14c) are linearly independent, uniformly in time, the vehicle-controller-estimator interconnection is locally asymptotically stable. Additionally, both the trajectory tracking and parameter estimation errors converge to zero and the linear and angular velocities are bounded.

This article has been accepted for inclusion in a future issue of this journal. Content is final as presented, with the exception of pagination.

Proof: The estimation errors of ζ_1 through ζ_6 are independent of the chosen controller and are globally exponentially stable. The parameters scaling the inputs, ζ_7 and ζ_8, are kept constant and guarantee that the controller is always well-defined as the inverse $\mathbf{B}^{-1}$ exists throughout the maneuver. From (23) and employing the same arguments as in Theorem 4 it follows that the velocities $\mathbf{v}$ and r are bounded for sufficiently small estimation errors. Since the estimator can run before the controller is active and is exponentially stable there is a time T after which the loop can be closed and the velocities remain bounded. The closed-loop system can be regarded as a perturbed system with state $(\mathbf{z}_1, \mathbf{z}_2)$ and perturbations $\tilde{\zeta}_1$ through $\tilde{\zeta}_6$. Since the velocities remain bounded for all time the perturbed system is locally Lipschitz in the state and perturbations. Recall the Lyapunov function (17) and its time derivative for the closed-loop system (27), as shown at the bottom of this page. To simplify the presentation of the final result consider

$$|\tilde{\zeta}| = \max(|\tilde{\zeta}_1|, |\tilde{\zeta}_2|, |\tilde{\zeta}_3|, |\tilde{\zeta}_4|, |\tilde{\zeta}_5|, |\tilde{\zeta}_6|)$$

and notice the definite positive function $W(\mathbf{z}_1, \mathbf{z}_2)$ is quadratic and is lower bounded by

$$W(\mathbf{z}_1, \mathbf{z}_2) \geq \bar{k}\|(\mathbf{z}_1, \mathbf{z}_2)\|^2$$

where the new gain $\bar{k} > 0$ depends on k_1, k_2, and β. An upper bound on the time derivative of the Lyapunov function can therefore be expressed as

$$\dot{V} \leq -\bar{k}\|(\mathbf{z}_1, \mathbf{z}_2)\|(\|(\mathbf{z}_1, \mathbf{z}_2)\| - B\tilde{\zeta})$$

where B is a positive constant. For sufficiently large tracking errors the time derivative is negative definite. We are then in the conditions of [10, Theorem 5.2] and the closed-loop system is locally ISS with respect to perturbations $(\tilde{\zeta}_1, \ldots, \tilde{\zeta}_6)$. Since the external perturbations arising from the estimation errors are exponentially stable, the interconnection of the estimator and controller is locally asymptotically stable. □

It should be noticed that the local-ISS property for the interconnected system from Theorem 5 is stronger than simply local asymptotic stability. Since the parameter errors converge exponentially, and independently of the convergence of the trajectory tracking errors, then if the estimator is allowed to be turned ON before the controller, there will always be a time T after which the parameters errors are sufficiently small and stability of the overall system can be achieved, for any initial conditions. Furthermore, if a good initial estimate is available for the unknown parameters then the initial parameters estimates can be chosen so that the interconnected system is within the region where the local-ISS property is verified, and then will remain there for all time.

VIII. Experimental Results

A. Numerical Simulations

The proposed integrated solution for trajectory tracking and online estimation was first tested in simulation to assess its viability for a real hovercraft model and to analyze the response of the ensemble controller and estimator to time-varying parameters. The trajectory tracking simulation is comprised of three distinct parts. First, the proposed controller is tested by considering that all the parameters are perfectly known and the trajectory tracking error is driven to zero. In the second part, starting at $t = 15$ s, the friction and viscous drag parameters for the hovercraft simulation are changed to half their initial value but the controller parameters are maintained. These parameters changes cause the trajectory tracking error to increase as there is a mismatch between the actual hovercraft dynamic coefficients and the ones assumed by the controller. Finally, at $t = 30$ s, the estimator is brought into the loop and the online parameters estimates are used for feedback by the controller. This greatly improves the performance of the overall system and the trajectory tracking error is brought to zero again. Vertical markers highlighting the phase commutations have been added to all the figures presented in Section VIII. The partition of the simulation experiment is summarized in Table I.

TABLE I
PARTITION OF THE NUMERICAL SIMULATION

Time (s)	System Dynamics	Controller Parameters	Estimator
0-15	Nominal	Nominal	—
15-30	Altered	Nominal	—
30-50	Altered	Estimator estimates	Active

The controller gains used for simulation are $k_1 = 2$ and $k_2 = 2$. The rudder arm is set at $a = 0.14$ (m) and the point of the vehicle that is tracking the trajectory is $\boldsymbol{\delta} = \begin{bmatrix}0.2 & 0\end{bmatrix}^T$ (m). The simulated vehicle mass and inertia are 0.585 (kg) and 0.01 (kg m), respectively. The parameter estimator was implemented as a Kalman filter for LTV systems with parameters $\mathbf{R} = 10^{-5}\mathbf{I}$ for the output noise covariance and $\mathbf{Q} = \text{diag}(10^{-4}\mathbf{I}_3, 10^{-2}\mathbf{I}_8)$ for the state disturbance covariance matrix. The covariances were chosen empirically based on the noise of each measured variable and tuned through repeated simulations. The reference trajectory for simulation is an ellipse described by

$$\mathbf{p}_d = \begin{bmatrix}1.5\sin(t) \\ 2.5\cos(t)\end{bmatrix}(m)$$

corresponding to a period of 2π s. A 2-D view of the reference and hovercraft trajectories is shown in Fig. 2. After an initial transient, the trajectory tracking performance is good and the hovercraft is brought to the reference trajectory. The modification of the simulation parameters at $t = 15$ s causes the trajectory tracking error to increase and the hovercraft follows an oval trajectory but with a larger radius than the reference, due to the mismatch between the parameters used for control and the actual parameters. Once the estimator is active in closed loop, at $t = 30s$, the hovercraft immediately steers toward the desired reference trajectory, which it then follows closely.

$$\dot{V} = -W(\mathbf{z}_1, \mathbf{z}_2) + (\beta\mathbf{z}_1 + \mathbf{z}_2)^T\mathbf{R}\begin{bmatrix}\zeta_7^{-1}(\tilde{\zeta}_1 \operatorname{sign} u + \tilde{\zeta}_2 u) \\ (\zeta_7 - \zeta_8\delta_x)^{-1}(\tilde{\zeta}_3 \operatorname{sign} v + \tilde{\zeta}_4 v + \tilde{\zeta}_5 \operatorname{sign} r\delta_x + \tilde{\zeta}_6 r\delta_x)\end{bmatrix} \tag{27}$$

This article has been accepted for inclusion in a future issue of this journal. Content is final as presented, with the exception of pagination.

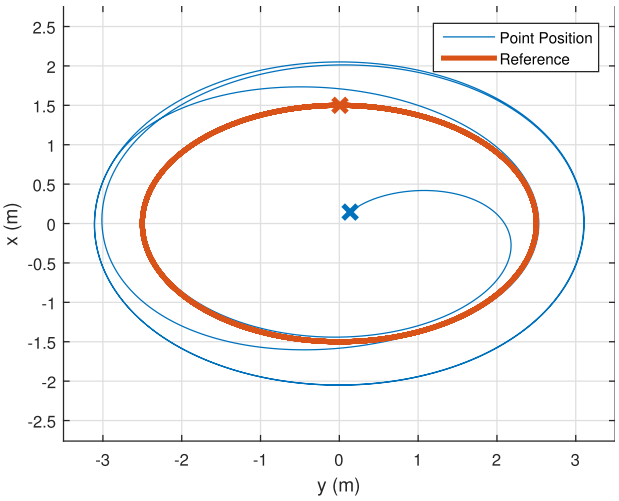

Fig. 2. Position of the hovercraft and reference position. The initial positions are marked with an $\times$.

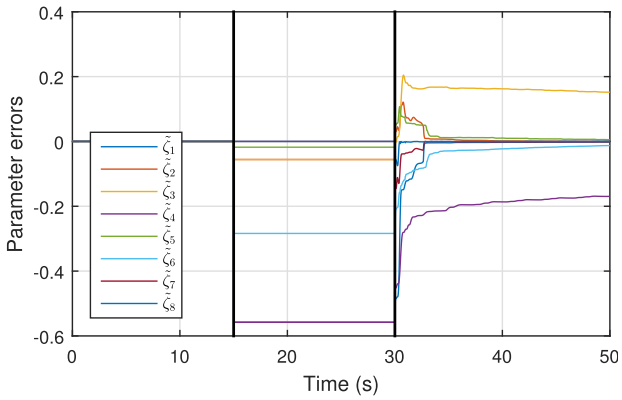

Fig. 3. Error of the online parameter estimation.

The parameter estimation error and the parameter estimates are presented in Figs. 3 and 4, respectively. The initial transient and the reaction to the parameter change are clearly visible in Fig. 3 when, at $t = 15$ s, the hovercraft's dynamics are modified so that all the friction and drag parameters vary instantaneously by 50%. At $t = 30$ s the estimator is brought online in closed loop with the controller and quickly adapts and tracks the correct parameters with the overall parameter error converging to zero.

It can be noticed in Fig. 3 that the convergence is considerably slower for parameters ζ_3 and ζ_4, associated with the lateral friction and linear drag coefficients. This happens because the chosen oval trajectory is not rich enough in lateral movements for the hovercraft and, as such, the adaptation of the parameters is slower. For trajectories where the relative orientation of the hovercraft and the trajectory has more variation the estimation of ζ_3 and ζ_4 will also converge faster to the real value.

The tracking errors during the simulation are presented in Fig. 5. When using the correct parameters the proposed controller performs well, with an initial transient that quickly vanishes. Once the hovercraft dynamics change, at $t = 15$ s, the controller no longer guarantees a zero tracking error and its performance worsens. During the parameter mismatch phase

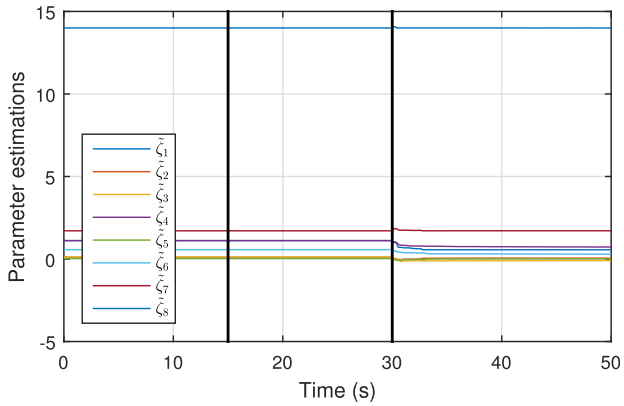

Fig. 4. Online parameter estimation.

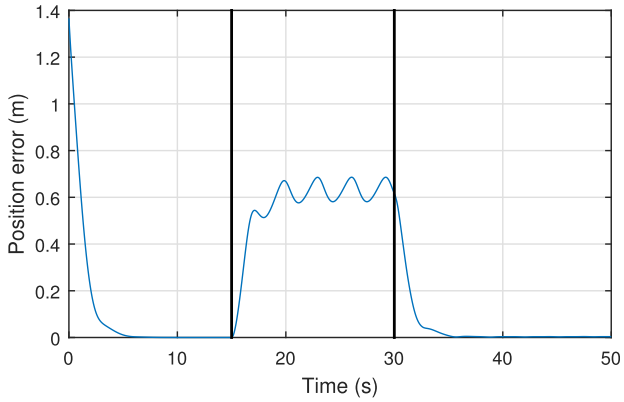

Fig. 5. Trajectory tracking error.

the tracking error enters a stable steady-state but the tracking error is high, around 60 cm. Finally, at $t = 30$ s, the controller loop is closed with the online estimates from the proposed estimator. Fed with more accurate parameter estimates the controller reduces the tracking error gradually to zero as the estimates also get more accurate, corroborating the result from Theorem 5.

Fig. 6 displays the hovercraft velocity during the trajectory tracking simulation. The ellipse maneuver is aggressive, in the sense that the velocity changes continuously and at a fast pace. Throughout the maneuver, even when the parameters estimator is running, the velocities are stable, as predicted by the result in Theorem 4.

For the sake of completeness, the actuation signals are shown in Figs. 7 and 8. From these figures it can easily be concluded that both thrust and rudder actuations are kept at reasonable values throughout all the maneuver.

B. Experimental Setup

Once the trajectory tracking controller and the parameter estimator have been assessed in simulation, the rapid prototyping and testing setup at the SCORE laboratory, University of Macau, was used to experimentally validate the proposed estimation and control laws. The experiments are developed in a MATLAB/Simulink environment that seamlessly integrates an optical motion capture system and radio communication with the vehicle. The integrated MATLAB

This article has been accepted for inclusion in a future issue of this journal. Content is final as presented, with the exception of pagination.

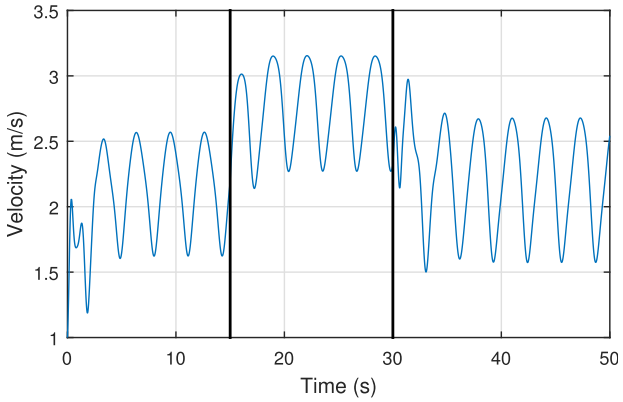

Fig. 6. Body velocity of the hovercraft.

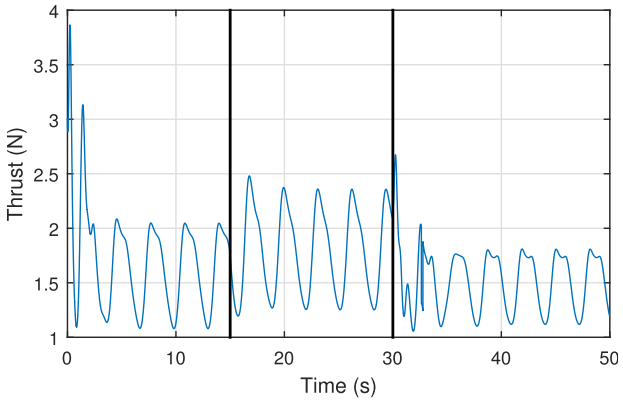

Fig. 7. Thrust actuation of the hovercraft.

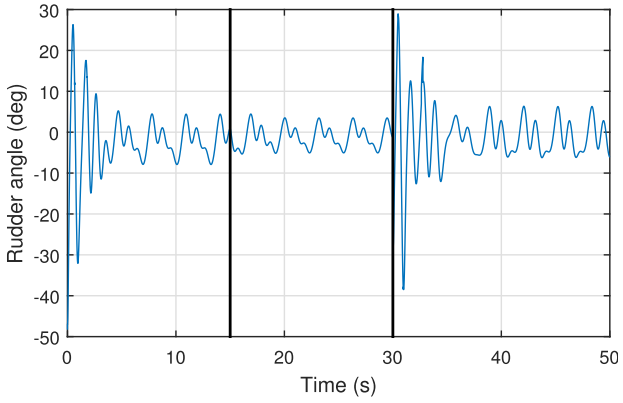

Fig. 8. Rudder actuation of the hovercraft.

environment allows for an effortless iteration from simulation to real experiments.

The vehicle used for the experiments is the radio controlled Ikarus hovercraft [11] depicted in Fig. 9. The vehicle has a length of 45 cm, a width of 25 cm, and a total weight of 585 g (batteries and RC receiver included). Two brushed motors move a continuous propeller that feeds the air cushion that lifts the hovercraft and a 130-mm propeller that generates the thrust force. The thrust force attacks a rudder located 16 cm behind the center of mass which is capable of reaching angles of $\pm 26°$. This hovercraft is very agile, readily available, and inexpensive, making it the ideal platform for this paper.

Fig. 9. Hovercraft with batteries, radio receiver, and motion capture markers.

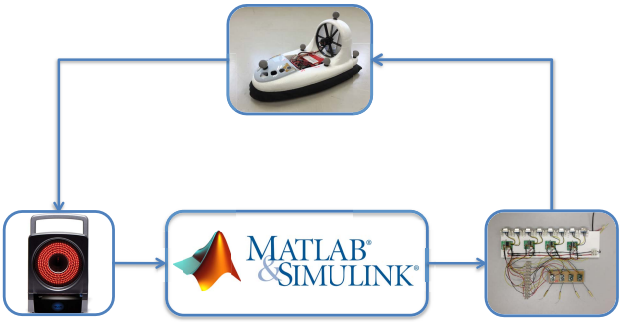

Fig. 10. Hovercraft integrated measurement and command architecture.

Due to the lack of payload for on-board sensors, the state of the vehicle must be estimated through external sensors. In our setup we use a VICON motion capture system [12], comprising 12 cameras, together with markers attached to the hovercraft. The set of markers is defined as a VICON object and accurate measurements are obtained for the vehicle's position and orientation. The performance of the motion capture system is such that the linear velocity can be well estimated from the position measurements by a simple backward Euler difference, with relatively low noise level. The state measurements from the motion capture system are obtained at 100 Hz.

We tested a scale model hovercraft on a laboratory setting as a proxy for a full scale hovercraft in an outdoor environment. In such conditions the attitude and angular rates are provided by an inertial measurement unit and the position and linear velocity are obtained via a global navigation satellite system, typically GPS. The use of carrier-phase enhancement solutions, such as GPS RTK, increases the typical position measurement accuracy of GPS from tens of meters to tens of centimeters and the linear velocity measurement accuracy to centimeters per second. This high accuracy allows the implementation of the proposed control solution in an outdoor environment without the use of an external camera setup. A navigation system can also be used to fuse GPS RTK measurements with the remaining inertial sensors, thereby providing even higher accuracy and lower noise levels.

A graphical representation of the overall architecture is presented in Fig. 10. We use two computer systems, one running the VICON motion tracking software and the Simulink model that generates the command signals sent to the other computer through Ethernet; and a second one that receives the command signals and sends them through serial port to the RF module at intervals of 22.5 ms. The decision to separate control and

This article has been accepted for inclusion in a future issue of this journal. Content is final as presented, with the exception of pagination.

TABLE II
PARTITION OF THE EXPERIMENTAL TEST

Time (s)	Dynamics	Controller Parameters	Estimator
0-30	Nominal	Nominal	—
30-60	Altered	Nominal	—
60-100	Altered	Estimates	Active

communications was made to avoid jitter in the transmission of the serial-port signals to the RF module, which occurs when running all the systems in the same computer, and leads to erratic communication with the vehicle.

C. Closed-Loop Estimation and Control

This section presents the experimental analysis of the trajectory tracking controller by itself and then introduces the proposed estimator in closed loop. For the experimental evaluation of the proposed controller we used an oval trajectory, with varying velocity, described as in the following equation and depicted in Fig. 12:

$$\mathbf{p}_d = \begin{bmatrix} 1.15\cos(0.7t) \\ 2.00\sin(0.7t) \end{bmatrix}.$$

The controller gains for the experimental run were adjusted to $k_1 = 1.75$, $k_2 = 1.5$, and the Kalman filter parameters of the estimator were $\mathbf{R} = \text{diag}(0.1,\ 0.1,\ 0.01)$ and $\mathbf{Q} = 0.1\mathbf{I}$. The parameters used when the estimator is not active were obtained using the proposed estimator on a prior run of the vehicle and are $\zeta_1 = 1.35, \zeta_2 = 0, \zeta_3 = 0, \zeta_4 = 1.20, \zeta_5 = 0.83, \zeta_6 = 0.48$ for the drag parameters and $\zeta_7 = 0.75, \zeta_8 = 3.66$ for the input coefficients, throughout all the maneuvers.

The maneuver was prepared as follows: the trajectory tracking controller is used with constant parameters for the initial section of the maneuver. At $t = 30$ s the drag conditions are modified by reducing the air flow in the air cushion supporting the hovercraft. Finally, at $t = 60$ s, the estimator is switched on and the parameters estimates are used for the trajectory tracking controller feedback. The time instants when the vehicle dynamics change and when the estimator is enabled are marked by vertical black bars in the figures. The portion of the experiment when the estimator is active is clearly visible in Fig. 11 as it corresponds to the interval where the estimates related to the drag coefficients are changing. A summary of the different experiment conditions is presented in Table II.

During the first 30 s of the experiment, the vehicle is sliding on a smooth uniform ground surface with a nominal air cushion pressure. This results in nominal constant drag coefficients and hence good results are obtained for tracking, with a mean error around 10 cm as confirmed by the position error plot in Fig. 13. When the air cushion pressure is reduced, from 30 to 60 s, the parameters are no longer adjusted to the vehicle reality and the position error increases to almost 20 cm. However, once the estimator is turned ON and connected in closed loop, from $t = 60$ s onward, the error is greatly reduced to under 5 cm, leading to better performance, even though the vehicle dynamics are now different due to the reduced airflow to the hovercraft skirt. Notice that the parameter adaptation

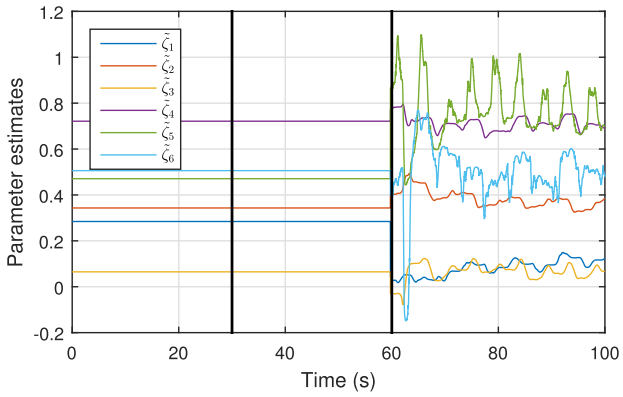

Fig. 11. Parameter estimation.

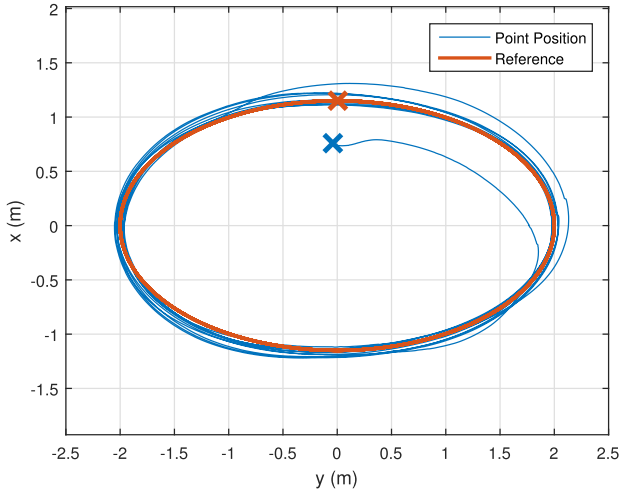

Fig. 12. Position of the delta point and reference position. The initial positions are marked with an $\times$.

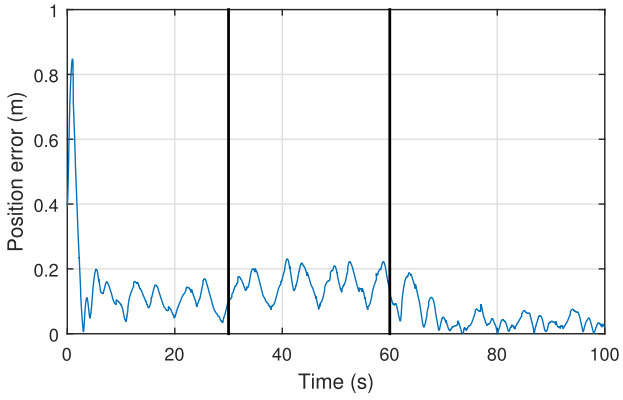

Fig. 13. Norm of the position error $\mathbf{z}_1$.

afforded by the estimator enables the closed-loop controller to outperform the nominal controller (without estimator) by adjusting even to the minute parameter variations arising from the small nonuniformities in the terrain surface.

The velocity profile of the vehicle during the maneuver is presented in Fig. 14 and varies substantially along each lap. The velocity is high for the proposed indoor application, allowing to explore the performance envelope of the vehicle, and its variation has the double advantage of forcing the thrust actuation to change during each lap and to allow all the

This article has been accepted for inclusion in a future issue of this journal. Content is final as presented, with the exception of pagination.

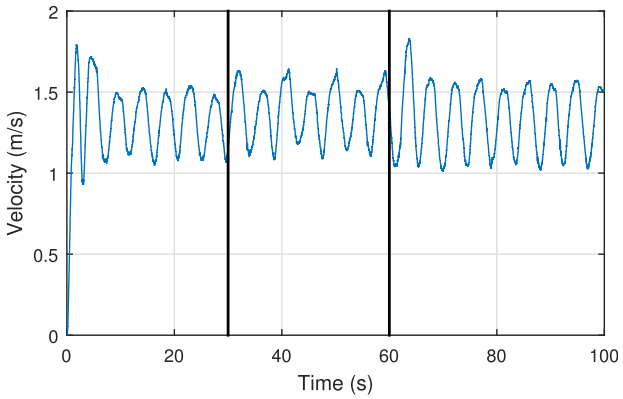

Fig. 14. Velocity profile of the trajectory.

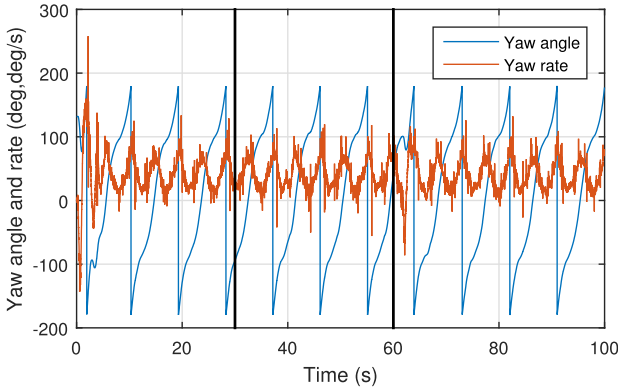

Fig. 15. Hovercraft's yaw angle and yaw rate.

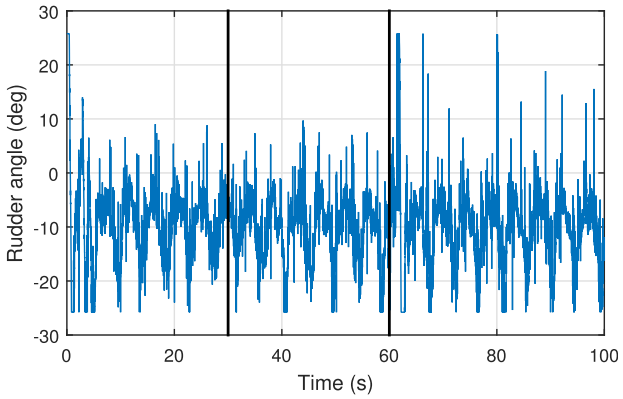

Fig. 16. Rudder actuation of the hovercraft.

parameters to be estimated since a changing velocity excites more of the estimator modes and makes the observability Grammian matrix positive definite.

The evolutions of the yaw angle and the respective rate, as well as the corresponding control actuation are shown in Figs. 15 and 16. The periodicity of the maneuver is clearly visible with the only exception being the initial transient when the vehicle is not close to the desired trajectory. The axis symmetry of the desired elliptical trajectory can also be observed in Fig. 15. During a complete lap (yaw angle changing by 360°) it can be noticed that the yaw rate comes close to zero twice and has two peaks. This cyclic change corresponds to the vehicle steering along the ellipse alternating between

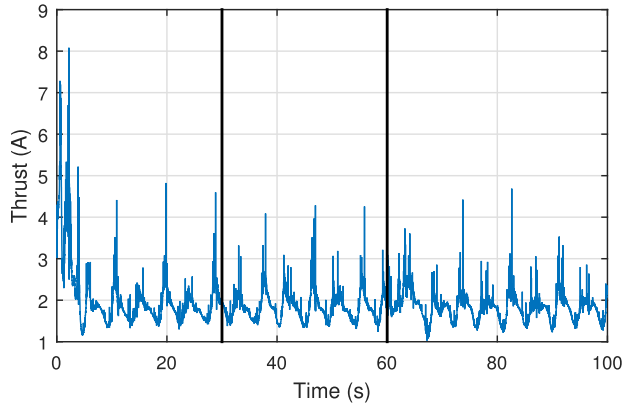

Fig. 17. Thrust actuation of the hovercraft.

moving along the long axis (lower curvature, lower yaw rate) and short axis (larger curvature, larger yaw rate). The evolution of the rudder angle follows closely the yaw rate, but with opposite signs, since large changes in heading require large rudder angles. The physical rudder angle saturates at $\pm 26°$, which is seldom attained.

The thrust command was identified by the current the propeller motor draws when running. The current is linearly related with the generated thrust force by the scaling coefficient b_T which is computed by the estimator. The thrust also evolves periodically and the commanded actuation, as seen in Fig. 17, is almost always below the physical motor limitation current of 6.1 A. Even in the nonideal conditions when the control parameters do not match reality both actuations are reasonably within their saturation limits and do not differ much from the nominal actuations. The higher periodic spikes in T, as well as the two outliers above 6.1 A, correspond to noisy measurements due to the vehicle crossing a region where it is less visible by the VICON motion capture system and the measurements are ill-conditioned and especially noisy.

It should also be noticed that the proposed controller is able to handle the measurement noise. The position and angle measurements are obtained by an optical motion capture system resulting in noise levels that are relatively low and comparable, at the same scale, with measurement noise from RTK GPS and attitude measurements obtained from an attitude and heading reference system. However, measurement noise is noticeable in the velocity states measurements, plotted in Figs. 14 and 15, since they are determined by a finite difference approximation wherein the high frequency noise is amplified.

IX. Conclusion

This paper presented an integrated parameter estimator and trajectory tracking controller for a nonholonomic hovercraft. A parameter estimator for generic time-varying systems that are linear in the unknown parameters was devised and then particularized for the vehicle at hand in order to estimate the unknown parameters related to the drag forces, inputs, mass, and inertia. A trajectory tracking controller was proposed for the hovercraft, which makes a fixed point in the body frame follow a predefined trajectory. The tracking error system is exponentially stable and its zero dynamics are stable.

This article has been accepted for inclusion in a future issue of this journal. Content is final as presented, with the exception of pagination.

Furthermore, the closed-loop interconnection of the estimator and controller was deemed to be locally asymptotically stable. The experimental results attested the stability of the interconnection as well as the performance and robustness of the proposed solution. The experimental results also corroborate that the introduction of the closed-loop parameter estimator greatly reduces the trajectory tracking error in non-nominal conditions without any adverse side effects. This greatly increases the performance of this kind of vehicle, which has the ability to move on very different surfaces that can drastically change the vehicle drag profile.

REFERENCES

[1] I. Fantoni, R. Lozano, F. Mazenc, and K. Y. Pettersen, "Stabilization of a nonlinear underactuated hovercraft," in *Proc. 38th IEEE Conf. Decision Control*, vol. 3. Dec. 1999, pp. 2533–2538.

[2] W. B. Dunbar, R. O. Saber, and R. M. Murray, "Nonlinear and cooperative control of multiple hovercraft with input constraints," in *Proc. IEEE Eur. Control Conf.*, Sep. 2003, pp. 1917–1922.

[3] A. P. Aguiar, L. Cremean, and J. P. Hespanha, "Position tracking for a nonlinear underactuated hovercraft: Controller design and experimental results," in *Proc. 42nd IEEE Conf. Decision Control*, vol. 4, Dec. 2003, pp. 3858–3863.

[4] K. Tanaka, M. Iwasaki, and H. O. Wang, "Switching control of an R/C hovercraft: Stabilization and smooth switching," *IEEE Trans. Syst., Man, Cybern. B, Cybern.*, vol. 31, no. 6, pp. 853–863, Dec. 2001.

[5] A. Stubbs, V. Vladimerou, A. T. Fulford, D. King, J. Strick, and G. E. Dullerud, "Multivehicle systems control over networks: A hovercraft testbed for networked and decentralized control," *IEEE Control Syst.*, vol. 26, no. 3, pp. 56–69, Jun. 2006.

[6] R. Munoz-Mansilla, D. Chaos, J. Aranda, and J. M. Diaz, "Application of quantitative feedback theory techniques for the control of a nonholonomic underactuated hovercraft," *IET Control Theory Appl.*, vol. 6, no. 14, pp. 2188–2197, Sep. 2012.

[7] P. Batista, C. Silvestre, and P. Oliveira, "Single range aided navigation and source localization: Observability and filter design," *Syst. Control Lett.*, vol. 60, no. 8, pp. 665–673, Aug. 2011.

[8] S. S. Sastry and C. A. Desoer, "The robustness of controllability and observability of linear time-varying systems," *IEEE Trans. Autom. Control*, vol. 27, no. 4, pp. 933–939, Aug. 1982.

[9] A. Jazwinski, "Stochastic processes and filtering theory," in *Mathematics in Science and Engineering*. Amsterdam, The Netherlands: Elsevier, 1970. [Online]. Available: https://books.google.co.uk/books?id=nGlSNvKyY2MC

[10] H. K. Khalil, *Nonlinear Systems*, 2nd ed. Englewood Cliffs, NJ, USA: Prentice-Hall, 1996.

[11] Ikarus. *Dragstair Hovercraft Instruction Manual and Specifications*. [Online]. Available: http://www.ikarus.net/download/anleitungen/Hovercrafts/Dragstair/dragstair_anleitung_3sprachig_incl_konformitt.pdf

[12] *VICON*. [Online]. Available: http://www.vicon.com

David Cabecinhas received the Licenciatura and Ph.D. degrees in electrical and computer engineering from the Instituto Superior Técnico, Lisbon, Portugal, in 2006 and 2014, respectively.

He has been a Researcher with the Institute for Systems and Robotics, LarSyS, Lisbon, since 2007. He is currently a Post-Doctoral Fellow with the Faculty of Science and Technology, University of Macau, Macau, China. His current research interests include nonlinear control, sensor-based and vision-based control with applications to autonomous aerial and surface vehicles, and the modeling and identification of aerial and surface vehicles.

Pedro Batista (M'10) received the Licenciatura degree in electrical and computer engineering in 2005 and the Ph.D. degree from the Instituto Superior Técnico (IST), Lisbon, Portugal, in 2005 and 2010, respectively.

From 2004 to 2006, he was a Monitor with the Department of Mathematics, IST. Since 2012, he has been with the Department of Electrical and Computer Engineering, IST, where he is currently an Assistant Professor. His current research interests include sensor-based navigation and the control of autonomous vehicles.

Dr. Batista has received the Diploma de Mérito twice during his graduation and his Ph.D. dissertation was awarded the Best Robotics Ph.D. Thesis Award by the Portuguese Society of Robotics.

Paulo Oliveira (S'91–M'95–SM'11) received the Licenciatura, M.Sc., and Ph.D. degrees in electrical and computer engineering from the Instituto Superior Técnico (IST), Lisbon, Portugal, in 1987, 1991, and 2002, respectively.

Since 2012, he has been an Associate Professor with the Department of Mechanical Engineering, IST. He has authored or co-authored over 65 journal papers and 180 conference communications. He has participated in more than 30 European and Portuguese research projects, over the last 25 years. His current research interests include autonomous robotic vehicles with a focus on the fields of estimation, sensor fusion, navigation, positioning, and mechatronics.

Carlos Silvestre (M'05) received the Licenciatura and M.Sc. degrees in electrical engineering, the Ph.D. degree in control science, and the Habilitation degree in electrical engineering and computers from the Instituto Superior Técnico (IST), Lisbon, Portugal, in 1987, 1991, 2000, and 2011, respectively.

Since 2000, he has been with the Department of Electrical Engineering, IST, where he is currently an Associate Professor of Control and Robotics, on leave. Since 2015, he has been a Professor with the Department of Electrical and Computers Engineering, Faculty of Science and Technology, University of Macau, Macau, China. Over the past years, he has conducted research on the subjects of the navigation guidance and control of air and underwater robots. His current research interests include linear and nonlinear control theory, the coordinated control of multiple vehicles, gain scheduled control, the integrated design of guidance and control systems, inertial navigation systems, and mission control and real-time architectures for complex autonomous systems with applications to unmanned air and underwater vehicles.